Structural stability of Lanthanum-based oxygen-deficient perovskites in redox catalysis: A density functional theory study

Qian Li[a], Yun-Xiang Deng[a], Yi-An Zhu[a,*], Yang Li[a], Zhi-Jun Sui[a], De Chen[b], Wei-Kang Yuan[a]

[a] UNILAB, State Key Laboratory of Chemical Engineering, Shanghai Key Laboratory of Multiphase Materials Chemical Engineering, East China University of Science and Technology, Shanghai, 200237, China
[b] Department of Chemical Engineering, Norwegian University of Science and Technology, N-7491, Trondheim, Norway

ARTICLE INFO

Keywords:
Perovskite
DFT
Oxygen vacancy
Structural stability
Reducibility

ABSTRACT

Periodic density functional theory calculations have been performed to examine the effect of oxygen deficiency on the structural stability of Lanthanum-based perovskites ($LaMO_3$), where on-site Coulomb interactions have been addressed by an additional Hubbard-type term. Calculated results indicate that with the exception of $LaFeO_3$, the oxygen vacancy formation energy ($\Delta E_{formation,vac}$) of $LaMO_3$ (M = Sc - Cu) becomes less positive when moving across the first transition metal period. The first four $LaMO_3$ perovskites have very high oxygen vacancy formation energies and can hardly be reduced under mild conditions, while the other five perovskites exhibit a much greater reducibility. During the formation of the first oxygen vacancy in $LaMO_3$ (M = Mn - Cu), the nearest neighbor transition-metal cations serve as the primary acceptors of the electrons left behind. As oxygen atoms are further removed, square-based pyramidal and tetrahedral coordination geometries appear successively, and an abrupt increase in $\Delta E_{formation,vac}$ is observed at a specific oxygen deficiency (δ), which defines the maximum possible δ in the perovskite structures. Under this definition, the M^{3+} cations (M = Mn - Ni) can be possibly reduced to M^{2+} while $LaCuO_3$ may lose at most one lattice oxygen atom per formula unit before it is deactivated.

1. Introduction

Perovskite-type oxides have a general empirical formula ABO_3, in which the A-site cation can be a rare earth, alkaline earth, or bismuth cation while the B-site cation usually comes from transition metal elements in periods 4, 5, and 6 of the periodic table [1]. Because of their tunable geometric and electronic structures, high chemical activity, high chemical stability, and low cost, perovskites have been extensively used in a wide range of technological applications, such as catalysts in heterogeneous catalysis [2], oxygen sources in membrane separation [3], cathode materials in solid oxide fuel cells (SOFCs) [4], and high-temperature oxygen sensors [5]. The interesting properties of perovskites can be attributed to the partially occupied d subshells of transition metal ions. Because transition metals often have more than one stable oxidation state, it is possible for perovskites to be oxidized or reduced under various reaction conditions. When applied in a reducing atmosphere, the perovskite materials are first left with surface oxygen vacancies and the transition metal cations in lower oxidation states. Then, the oxygen vacancies are attacked by O_2 molecules in the overlying gas, which is chemisorbed as oxygen ions, thus reforming the catalyst. This sequence of events follows the Mars van Krevelen mechanism, sometimes involving the collapse of the perovskite structures under strain and stress.

Perovskites have long been proposed as potential substitutes for noble metals in redox reactions [2]. For instance, they can be used as an effective catalyst for partial oxidation of methane by chemical looping, achieving a high conversion of methane and a high selectivity toward carbon monoxide [6,7]. As an oxygen carrier, perovskites-type oxides react with methane with lattice O ions present in the bulk, resulting in the formation of oxygen vacancies. On the one hand, this method provides an alternative way to the usage of pure oxygen obtained from high-cost air separation. On the other hand, the existence of oxygen vacancies in oxides would significantly affect the physical and chemical properties of perovskites, and more importantly, affect the stability of perovskites. With the reduction proceeding, oxygen vacancies successively accumulate. Once the oxygen concentration is lowered to a certain degree, perovskites would decompose into mixed oxides, leading to carbon deposition and catalyst deactivation.

As another example, perovskite-types oxides are promising candidates for cathode materials in developing intermediate- or low-temperature SOFCs operating at 500–800 °C due to their good electronic and ionic conductivity as well as a high catalytic activity for oxygen

Table 1
Electronic, magnetic, and crystal structures of $LaMO_3$ perovskites.

	$LaScO_3$	$LaTiO_3$	$LaVO_3$	$LaCrO_3$	$LaMnO_3$	$LaFeO_3$	$LaCoO_3$	$LaNiO_3$	$LaCuO_3$
PAW potential	La O_s Sc_sv	Ti_pv	V_sv	Cr_pv	Mn_pv	Fe_pv	Co	Ni_pv	Cu
Valence electron configuration	$5s^2\ 5p^6\ 6s^2\ 5d^1$ $2s^2\ 2p^4$ $3s^2\ 3p^6\ 4s^2\ 3d^1$	$3p^6\ 3d^2\ 4s^2$	$3s^2\ 3p^6\ 3d^3\ 4s^2$	$3p^6\ 3d^5\ 4s^1$	$3p^6\ 3d^5\ 4s^2$	$3p^6\ 3d^6\ 4s^2$	$3d^7\ 4s^2$	$3p^6\ 3d^8\ 4s^2$	$3d^9\ 4s^2$
U_{eff}	0	1.3	3.0	3.0	4.7	4.8	4.2	7.0	4.5
Magnetic structure	NM	GAFM	CAFM	GAFM	AAFM	GAFM	FM	FM	NM
Crystal structure	*Pbnm*	*Pbnm*	*Pbnm*	*Pbnm*	*Pbnm*	*Pbnm*	$R\bar{3}c$	$R\bar{3}c$	$R\bar{3}c$

reduction reaction (ORR) [8,9]. Appropriate concentration of oxygen vacancies within the bulk cathode material is the key to fast ionic conductivity and ORR rates [9]. Unfortunately, the non-stoichiometric perovskite-types oxides present in the SOFC cathodes also suffer from the phase transition to binary metal oxides with the formation of grain boundaries [10]. Nakamura et al. [11] studied the structural evolution of a series of $LaMO_3$ (M = V, Cr, Mn, Fe, Co, and Ni) oxides upon H_2 reduction at 1273 K. The perovskites containing reducible transition metal ions underwent important crystalline and chemical transformations at certain oxygen partial pressures. A similar and undesirable phase transition was also found to happen in some complex perovskites upon temperature-programmed reduction (TPR), such as in $La_{0.8}Sr_{0.2}Co_{0.4}Fe_{0.6}$ that is widely used in cathode materials in SOFCs.

The phase separation in perovskites would significantly impede the supply of lattice oxygen and impair the catalytic activity, thus limiting their commercial applications. Therefore, it is important to examine how the structural stability of perovskites would vary with the oxygen content in bulk oxide. Of particular interest is whether there exists a maximum possible oxygen deficiency (δ_{max}) at which non-stoichiometric $ABO_{3-\delta}$ perovskites may possibly maintain a stable crystal structure. Here the oxygen deficiency (δ) increases with successive oxygen removal and can be defined as the degree of oxygen loss. The determination of the maximum possible oxygen deficiency could facilitate the determination of the operating conditions, e.g., the reduction time and oxidation time of perovskites in chemical looping, thus achieving a good catalyst reproducibility and long-term stability.

In this regard, many experimental attempts have been made to determine the oxygen deficiency in perovskite-type oxides [12–15]. It was reported through thermal gravimetric analysis that the oxygen deficiency in $BaFeO_{3-\delta}$ could be increased to as high as 0.58 at 700 °C [16]. Actually, a good many of $ABO_{3-\delta}$ perovskites may have a deviation of ~0.5 from the oxygen stoichiometry [12]. However, after doped with some other elements, perovskite-type oxides may have a much higher oxygen deficiency (e.g., δ = 0.7 in $Ba_{0.5}Sr_{0.5}Co_{0.8}Fe_{0.2}O_{3-\delta}$ [17] and δ = 0.75 in $YBa_2Cu_3O_{6.75}$ [18]).

Although the structural stability of oxygen-deficient perovskites has been the subject of many experimental research studies, so far there is no comprehensive theoretical work concerning the reason why the experimentally measured oxygen deficiency varies from perovskite to perovskite. By using the density functional theory (DFT) and DFT + U approaches, Zhang et al. [19] calculated the oxygen vacancy formation energy in barium-strontium-cobalt-ferrite (BSCF) over a range of oxygen deficiencies ($0.125 \le \delta \le 0.875$), but the structural stability of BSCF has not been discussed in terms of its oxygen content. In this contribution, DFT + U calculations have been carried out to examine the reducibility and structural stability of stoichiometric and oxygen-deficient $LaMO_3$ (M = Sc - Cu) perovskites. First, the formation energy of the first oxygen vacancy is calculated and used as a measure of the reducibility of $LaMO_3$, which is then decomposed into bonding energy and distortion energy to identify the key factor that determines the interaction between transition metal cations and oxygen anions. After that, electronic structure analysis is carried out to reveal the charge redistribution upon oxygen vacancy formation. Next, the energetics and structural evolution accompanying the successive oxygen removal are discussed, and the maximum possible oxygen deficiency for each $LaMO_3$ is determined and compared with available experimental observations. Finally, we conclude by discussing the implication of our results in the potential application of perovskites in the field of redox catalysis.

2. Computational details

Our electronic structure calculations were carried out using the VASP package [20,21], in which the Perdew-Burke-Ernzerhof (PBE) functional [22] was used to treat the exchange and correlation of the Kohn-Sham theory and the projector-augmented wave (PAW) method [23] was employed to represent the interactions between ion cores and valence electrons. In addition to the PBE functional, the BEEF-vdW functional [24] that may approximately account for London dispersion forces has also been used as a first test of our methods. It was found that the difference in the calculated energetics between these two functionals is less than 0.2 eV, which falls well within the inherent uncertainty of DFT calculations. Thus, the PBE functional can predict with reasonable accuracy the structure and energy of the $LaMO_3$ perovskites. Since standard exchange-correlation functionals suffer from the "self-interaction error" that leads to excessive electron delocalization, an additional Hubbard-type term was applied in the DFT + U method [25,26] to address the on-site Coulomb interactions between the localized transition metal *d* states. By using the "hard" PAW potentials, a plane-wave energy cutoff of up to 600 eV was necessary to converge the total energy per atom in $LaMO_3$ to within 1 meV. The effective U (U_{eff}) values and PAW potentials (including the valence electron configurations) used in this work are summarized in Table 1. Sampling of the Brillouin zone was performed with the Monkhorst-Pack method [27] and electronic occupancies were determined according to the Gaussian scheme with an energy smearing of 0.1 eV. For the majority of this study, spin-polarized calculations were performed to obtain reasonably accurate structures and energetics, where experimentally observed magnetic configurations were adopted. For example, it was reported that $LaCoO_3$ exhibits great magnetic complexity and has its ground state in the intermediate-spin state [28], which was thus considered in our calculations. The effect of magnetism was not included in the calculations of $LaScO_3$ and $LaCuO_3$ because in our preliminary test the energetics of these two perovskites were found to be independent of the spin state. The magnetic and crystal structures of the transition metal-based perovskites are also included in Table 1. Energy minimization of stoichiometric perovskites was first conducted with both the atomic coordinates and lattice vectors allowed to relax. Then, with the cell parameters kept fixed at their equilibrium values, the positions of atoms involved in the oxygen-deficient perovskites are optimized until the forces on each atom are less than 0.03 eV/Å.

It was reported that ideal cubic perovskites are only stable at extremely high temperatures while under mild conditions $LaMO_3$ perovskites may adopt either an orthorhombic (M = Sc - Fe) or a

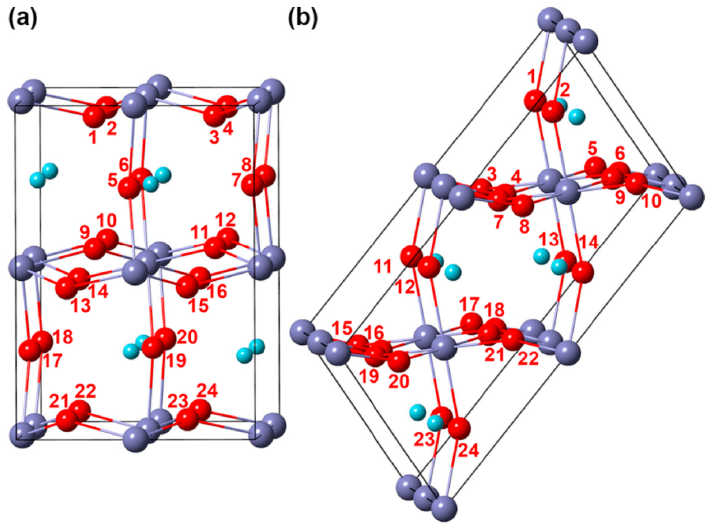

Fig. 1. Schematic representations of $LaMO_3$ perovskites adopting (a) an orthorhombic (M = Sc - Fe) and (b) a rhombohedral (M = Co - Cu) structure. The cyan and royal balls represent the La and M cations, respectively, and the O anions are colored red and labelled with the serial number (For interpretation of the references to colour in this figure legend, the reader is referred to the web version of this article).

rhombohedral structure (M = Co - Cu), with a *Pbnm* or a $R\bar{3}c$ space group [1]. In order to examine how the structural stability of oxygen-deficient perovskites may vary with the oxygen content in bulk oxides, the crystal structures of $LaMO_3$ (M = Sc - Fe) and $LaMO_3$ (M = Co - Cu) were represented as a $2 \times 1 \times 1$ and a $2 \times 2 \times 1$ supercell of their respective primitive cells (see Fig. 1), both of which consisting of 24 oxygen ions and having 8 formula units. A $3 \times 5 \times 5$ Monkhorst-Pack grid was used for k-point sampling in Brillouin zone of the supercells. For ease to note and clarity, the oxygen ions that could be removed from the bulk of perovskites are labelled in Fig. 1 with the serial number.

From Fig. 1(a), one can see that according to the atomic environment these oxygen ions can be classified into two categories, one in the MO_2 layer (called equatorial O, e.g., O1) and the other in the LaO layer (called apical O, e.g., O5). However, as the oxygen ions are successively removed, the symmetry of the crystal structures is lowered and eventually broken. For example, after the O5 ion is first abstracted from the orthorhombic structure, the system no longer belongs to the space group *Pbnm* and there exist 15 possible configurations for the subsequent oxygen removal. If one continues to create more vacancies in $LaMO_3$, there would be no oxygen ion that is equivalent to one another, making the situation quite complex. For this reason, we used the most and second most stable configurations at a specific oxygen deficiency as the starting point to identify the most and second most stable configurations at a higher concentration of oxygen vacancies, in much the same way as that proposed by Zhang et al. [19]. This procedure was repeated until 10 vacancies are formed in bulk oxide, giving rise to the maximum oxygen deficiency of 1.25. As for the perovskites adopting the rhombohedral structure, the only difference is that all the oxygen ions involved in the lattice are equivalent [see Fig. 1(b)] and, consequently, there is only one choice available for removing the first oxygen vacancy.

3. Results and discussion

3.1. Reducibility of $LaMO_3$

3.1.1. Oxygen vacancy formation energy

In perovskite-catalyzed redox reactions, electron transfer is accompanied by the oxidation of surface oxygen ions to yield gas-phase oxygen-containing species and surface oxygen vacancies. Driven by the oxygen concentration gradient established across catalyst particles, transport of oxygen ions from the bulk oxide to the oxide surface would take place. Hence, the reducibility of perovskites that is closely related to their elemental compositions plays a key role in determining the catalytic properties, such as vacancy concentration and oxygen mobility. To estimate how readily $LaMO_3$ perovskites may donate an oxygen ion, the formation energy ($\Delta E_{formation,vac}$) of the first oxygen vacancy in bulk oxide was defined as

$$\Delta E_{formation,vac} = E_{defective} + \frac{1}{2}E_{O_2} - E_{perfect} \quad (1)$$

where $E_{perfect}$ and $E_{defective}$ are the total energies of the stoichiometric $LaMO_3$ and the defective $LaMO_3$ with one oxygen vacancy formed, respectively, and E_{O_2} is the total energy of an O_2 molecule in its lowest-energy triplet state. Under such a definition, a positive value is indicative of an energy-gain process. Since DFT-GGA would significantly overestimate the binding strength of O_2 molecules, a correction needs to be made to its total energy. Unless otherwise specified, the calculated oxygen vacancy formation energies in this work have been corrected and increased by 0.42 eV per oxygen vacancy for $LaScO_3$, $LaTiO_3$, $LaCrO_3$, $LaMnO_3$, $LaFeO_3$, $LaCoO_3$, and $LaNiO_3$, and by 0.37 eV per oxygen vacancy for $LaVO_3$ and $LaCuO_3$. The details of the derivation of these correction values are given in the Supporting Information.

The calculated oxygen vacancy formation energies in $LaMO_3$ are presented in Fig. 2(a). It is well accepted that this quantity can be used as a measure of the reducibility of $LaMO_3$ perovskites [2]. The lower the oxygen vacancy formation energy, the more readily the transition metal ions can be reduced. From the figure, it is clear that with the exception of $LaFeO_3$, the oxygen vacancy formation energy becomes less positive on moving from $LaScO_3$ to $LaCuO_3$, indicating an increased reducibility. The reason why Fe^{3+} is even harder to be reduced than Mn^{3+} lies in the fact that Fe^{3+} has a very stable half-filled 3d subshell and the reduction of Mn^{3+} to Mn^{2+} is energetically very favorable. The electron left behind when the oxygen vacancy is formed is localized on the Fe cation, which would add an antiparallel spin and provide no extra exchange stabilization [9]. Therefore, the rise in the $\Delta E_{formation,vac}$ of $LaFeO_3$ is due to the additional electron-electron repulsion in the doubly occupied d-orbital.

For the first four $LaMO_3$ perovskites, although the oxygen vacancy formation energy decreases dramatically with increasing the atomic number, the calculated value for $LaCrO_3$ is still fairly high (> 5.5 eV), which implies that these perovskite-type oxides are quite difficult to reduce. It is therefore not surprising that they exhibit poor performance in experiment and are rarely used as catalysts in redox reactions. For

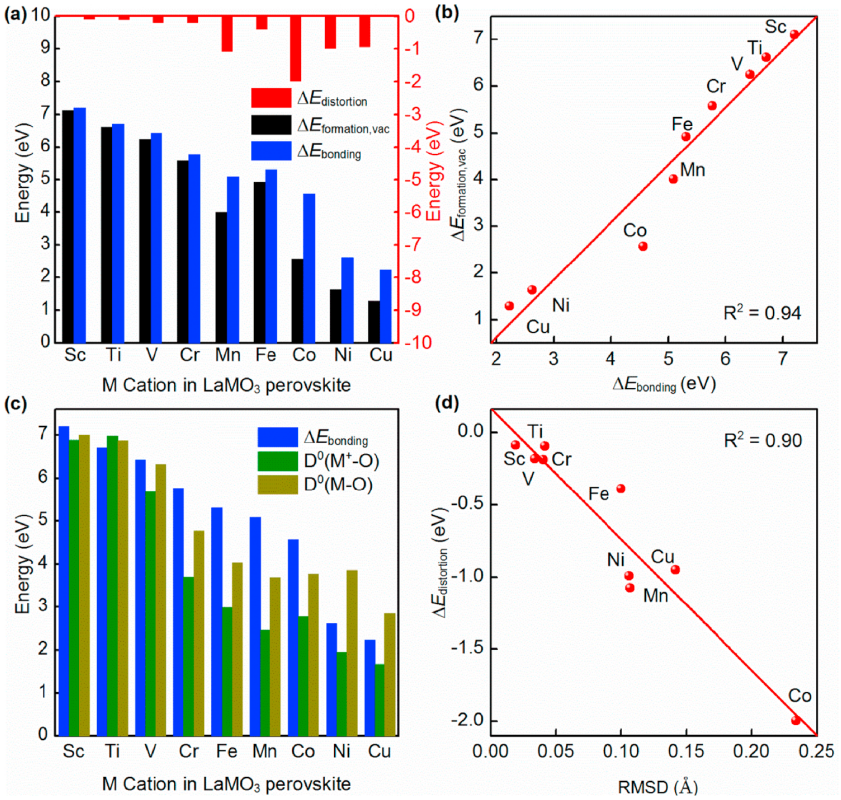

Fig. 2. (a) Decomposition of oxygen vacancy formation energy of $LaMO_3$ (M = Sc - Cu) into bonding energy and distortion energy; (b) linear scaling relation between oxygen vacancy formation energy and bonding energy; (c) comparison between bonding energy and experimentally measured bond dissociation energy of diatomic species; (d) plot of distortion energy against RMSD of the ions during oxygen vacancy formation.

instance, Nomura and his co-workers found the chemical reactivity of $LaScO_3$ powders is very low even at a high temperature of 1873 K [29]. Van Grieken et al. [30] reported that $LaTiO_3$ exhibits low activity and selectivity for the conversion of CO to methanol. When Cu is substituted partially for Ti, however, the catalytic performance is substantially increased. Tascón et al. [14] used $LaVO_3$ and $LaCrO_3$ as catalysts for CO oxidation and found that the catalytic activity of $LaVO_3$ is nearly zero and that of $LaCrO_3$ is only 0.4×10^{-7} mol CO converted $m^{-2} s^{-1}$ at 600 K.

By comparison, the oxygen vacancy formation energies of $LaMO_3$ (M = Mn - Cu) are below 5 eV and a marked decrease is observed, indicating a much higher reducibility. Experimentally, these more easily reduced perovskite oxides are highly active catalysts in heterogeneous catalysis, which can be seen from their superior catalytic performance in redox reactions. For example, Royer and Duprez [31] suggested that manganite and cobaltite perovskites are very active for CO oxidation. $LaFeO_3$ perovskites are attractive candidates as oxygen carriers and catalysts for partial oxidation of methane toward CO and H_2 by chemical looping reforming [32]. $LaNiO_3$ are potential oxidation catalysts and promising candidates for the steam reforming reaction.

3.1.2. Bonding energy and distortion energy

To identify the key factor that determines the variation of the $\Delta E_{formation,vac}$ as the transition metal element is changed, the formation of oxygen vacancies can be thought of as taking place in two successive steps: (i) removal of an oxygen atom while the crystal structure is kept constrained and (ii) relaxation of the structure in the presence of the oxygen vacancy. Accordingly, the $\Delta E_{formation,vac}$ can be decomposed into two contributions:

$$\Delta E_{formation,vac} = \Delta E_{bonding} + \Delta E_{distortion} \quad (2)$$

Where

$$\Delta E_{bonding} = E_{defective}^{constrained} + \frac{1}{2}E_{O_2} - E_{perfect} \quad (3)$$

and

$$\Delta E_{distortion} = E_{defective} - E_{defective}^{constrained} \quad (4)$$

and $E_{defective}^{constrained}$ is the single-point energy of oxygen-deficient $LaMO_3$ without any geometry optimization. Under this definition, the bonding energy ($\Delta E_{bonding}$) is a measure of how strongly the transition metal cations and oxygen anions interact with each other, and the distortion energy ($\Delta E_{distortion}$) can be used to estimate the energy gained from the crystal structural relaxation upon formation of the oxygen vacancy.

The calculated $\Delta E_{bonding}$ and $\Delta E_{distortion}$ are also given in Fig. 2(a). From the figure, one can see that the $\Delta E_{bonding}$ and $\Delta E_{distortion}$ have a positive and a negative value, respectively, and the latter has a relatively small magnitude that is below 1.10 eV for most of the perovskites. The only exception is $LaCoO_3$, the structure of which would release more than 2.00 eV of heat to relieve strain. This seems to be associated with the intermediate spin state of the Co cations and the Jahn-Teller distortion of the MO_6 octahedra that have been observed both theoretically and experimentally [33,34]. The calculated $\Delta E_{bonding}$ varies in much the same way as the $\Delta E_{formation,vac}$, indicating that a significant amount of energy is required to break the M–O bond and the variation in $\Delta E_{formation,vac}$ is dominated by the variation in $\Delta E_{bonding}$. Actually, there exists a good linear correlation between $\Delta E_{formation,vac}$ and $\Delta E_{bonding}$, as can be seen in Fig. 2(b). This conclusion is consistent with the study by Pavone et al. [9] who claimed that the reduction in $\Delta E_{formation,vac}$ along the period can be explained by the decreased intrinsic strength of the metal-oxygen bond and the exception of $LaFeO_3$ is caused by the absence of the extra stabilization arising from the intra-

atomic exchange energy. In Fig. 2(c), the calculated $\Delta E_{bonding}$ is compared with the experimentally measured bond dissociation energies of the diatomic M–O and M^+-O (M = Sc - Cu) at 0 K [35–37]. It shows clearly that these three quantities follow almost the same trend except that the Co/Co^+-O bond has a slightly higher bonding energy than the Mn/Mn^+-O bond in the diatomic species, which could be probably due to the different oxidation states of the transition metals in the three types of substances.

After an O atom is removed from the oxide matrix, the atoms remaining in the lattice would fully relax to relieve the strain and stress. Therefore, it is reasonable to expect that the distortion energy is dependent strongly on the displacement of the remaining atoms. Our calculated results indicate that for most of the $LaMO_3$ perovskites the La and M cations are displaced by less than 0.02 Å. Thus, only the displacement of the remaining O atoms in the defective $LaMO_3$ was considered in this work and their root mean squared displacement (RMSD) upon formation of an oxygen vacancy was calculated as

$$RMSD = \sqrt{\frac{1}{n}\sum_{i=1}^{n}(r_i - r_i^0)^2} \quad (5)$$

where n represents the number of O atoms in the defective $LaMO_3$, r_i^0 and r_i are the positions of the remaining O atoms before and after the oxygen removal, respectively. In Fig. 2(d), the calculated distortion energy is plotted as a function of the RMSD of the remaining 23 O atoms. It can be seen that for the early transition metal-based perovskites the RMSD varies from 0.02 to 0.04 Å while the data for the late transition metal-based perovskites lie in the range 0.10–0.23 Å, and, more importantly, a straight line fits the data very well, confirming that the RMSD can be used to gauge the degree of distortion upon oxygen vacancy formation.

3.1.3. Electronic structure analysis

Electronic structure analysis allows us to examine more closely the chemical bonding between La, M, and O in perovskites. Bader's theory [38], which is based on the concept of a gradient vector path, provides a rigorous way of partitioning the total electron density into atomic contributions and makes it possible to quantitatively represent the polarity of chemical bonds in molecules and solids. The calculated effective Bader charges on La, M, and O in stoichiometric $LaMO_3$ (M = Sc - Cu) are listed in Table 2. The results indicate that the bonding in perovskites have some covalent character, and because the effective Bader charges on the transition metal atoms are less positive than those on La, there is less ionic contribution to the M—O bonding than to the La—O bonding. In addition, the effective Bader charges on the transition metals decrease considerably as we move from Sc to Cu, whereas the charges on La have almost the same values in different perovskites, implying that the M—O bonding becomes less polarized with increasing the atomic number of the transition metal and the identity of the M cation has a negligible effect on the degree of covalency in the La—O bonds.

In order to shed light on the electron density redistribution upon formation of oxygen vacancy, Bader's analysis was also performed for defective $LaMO_3$ as well. When an oxygen vacancy is present, the electrons that are left behind will be transferred to the remaining ions in bulk oxide. The percentages of the electrons accepted by each element in $LaMO_3$ are presented in Fig. 3. As can be seen from the figure, more than 50% (52%–78%) electrons are transferred to the M cations in

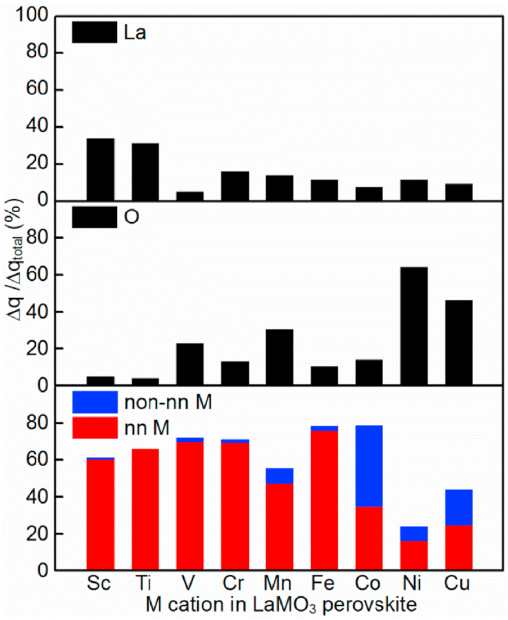

Fig. 3. Percentages of electrons accepted by each element in $LaMO_3$ upon oxygen vacancy formation.

$LaMO_3$ (M = Sc - Co), while for $LaNiO_3$ and $LaCuO_3$ the O anions become the primary electron acceptor. If we further divide the M cations into two groups, the nearest neighbor (nn) M cations to the vacancy and non-nearest neighbor (non-nn) cations, the nn M cations are found to be reduced most significantly except for those in $LaMnO_3$, although in $LaMO_3$ (M = Co - Cu) the charge redistribution has already become very delocalized. The even more dramatic delocalization in LaMnO3 can be explained by superexchange model [39], where the hopping of electrons from Mn^{2+} to Mn^{3+} via oxygen ion, and hence the Mn^{2+} and Mn^{3+} ion exchange, takes place.

3.2. Structural stability of oxygen-deficient $LaMO_3$

3.2.1. Formation energy of multiple oxygen vacancies in $LaFeO_3$

In order to meet the requirements of the catalysts for redox reactions, perovskites need to have a good structural stability even if a considerable amount of lattice oxygen atoms are removed from their bulk structures. Hence, the question that now arises is whether there exists a maximum possible oxygen deficiency beyond which $LaMO_3$ may no more retain the stable crystal structure. Although some progress toward this problem has already been made in the laboratory, it remains challenging to characterize the detailed structure and composition of perovskites, especially when multiple oxygen vacancies are introduced into bulk oxide.

Quantum chemical calculations are of extraordinary power in this regard. Here the formation energy of the 8δ-th oxygen vacancy can be calculated as

Table 2
Calculated effective Bader charges on La, M, and O in $LaMO_3$ (M = Sc - Cu).

	$LaScO_3$	$LaTiO_3$	$LaVO_3$	$LaCrO_3$	$LaMnO_3$	$LaFeO_3$	$LaCoO_3$	$LaNiO_3$	$LaCuO_3$
$q_{La}/(\|e\|)$	2.05+	2.03+	2.07+	2.08+	2.09+	2.08+	2.09+	2.10+	2.10+
$q_M/(\|e\|)$	2.00+	1.94+	1.89+	1.76+	1.72+	1.78+	1.46+	1.33+	1.15+
$q_O/(\|e\|)$	1.35-	1.33-	1.31-	1.27-	1.28-	1.29-	1.21-	1.14-	1.08-

Table 3
Formation energy per oxygen vacancy ($\Delta E^{\delta}_{formation,vac}$) in $LaFeO_{3-\delta}$.

δ	V1	V2	V3	V4	V5	V6	V7	V8	V9	V10	$\Delta E^{\delta}_{formation,vac}$ (eV)
0.125	**O1**										**4.85**
	O5										4.92
0.25	**O5**	**O19**									**4.06**
	O5	O7									4.59
0.375	**O5**	**O19**	**O16**								**4.30**
	O5	O19	O24								4.30
0.5	**O5**	**O19**	**O16**	**O3**							**4.18**
	O5	O19	O24	O10							4.28
0.625	**O5**	**O19**	**O16**	**O3**	**O21**						**5.22**
	O5	O19	O16	O3	O6						5.30
0.75	**O5**	**O19**	**O16**	**O3**	**O21**	**O10**					**5.22**
	O5	O19	O16	O3	O21	O24					5.36
0.875	**O5**	**O19**	**O16**	**O3**	**O21**	**O10**	**O13**				**5.36**
	O5	O19	O16	O3	O21	O10	O14				5.40
1.00	**O5**	**O19**	**O16**	**O3**	**O22**	**O12**	**O13**	**O12**			**5.55**
	O5	O19	O16	O3	O22	O12	O13	O2			5.55
1.125	**O5**	**O19**	**O16**	**O3**	**O22**	**O12**	**O13**	**O12**	**O24**		**5.51**
	O5	O19	O16	O3	O22	O12	O13	O2	O24		5.62
1.25	**O5**	**O19**	**O16**	**O3**	**O22**	**O12**	**O13**	**O12**	**O24**	**O18**	**5.51**
	O5	O19	O16	O3	O22	O12	O13	O12	O24	O11	5.64

$$\Delta E^{\delta}_{formation,vac} = E^{8\delta}_{defective} + \frac{1}{2}E_{O_2} - E^{8\delta-1}_{defective} \quad (6)$$

where $E^{8\delta}_{defective}$ and $E^{8\delta-1}_{defective}$ are the total energies of oxygen-deficient $LaMO_{3-\delta}$ with 8δ and 8δ-1 oxygen vacancies, respectively. The formation energy per oxygen vacancy obtained from the most or second most stable $LaFeO_{3-\delta}$ configurations is listed in Table 3, where Vn represents the n-th oxygen vacancy and the serial number of the oxygen atom is defined in Fig. 1. The corresponding data for the other eight $LaMO_{3-\delta}$ can be found in the Supporting Information. It should be noted that the ordered superstructures that are often formed at very low temperatures were not considered in this work because an increase in temperature would lead to an entropy increase and the disordered non-stoichiometric phases typically prevail [40].

From the table, one can see that the energies required to remove the first oxygen atom from $LaFeO_3$ are 4.85 eV and 4.92 eV at the O1 and O5 sites, respectively; that is, removing an equatorial O atom is energetically more favorable. Given the fact that the energy difference is very small, we used both of the two $LaMO_{2.875}$ configurations as the starting point to search for the lowest-energy configuration at the oxygen deficiency of 0.25. It is interesting to find that the most stable $LaFeO_{2.75}$ configuration is derived by removing an additional oxygen atom in the second most stable $LaFeO_{2.875}$, and the formation energy of other oxygen vacancies is at least 0.5 eV higher; that is, the lowest-energy configuration at a specific oxygen deficiency does not necessarily result from lowest-energy configuration with a higher concentration of oxygen atoms. The energies associated with the removal of the second, third, and fourth oxygen atoms are quite close and fall in the range 3.98–4.22 eV. However, when the oxygen deficiency is increased to 0.625 (i.e., the fifth oxygen atom is removed from the system), the oxygen vacancy formation energy rises sharply to 5.14 eV, implying that there is too much energy needed to remove the fifth oxygen atom and the framework might have collapsed at such an oxygen deficiency. If we continue to abstract another five oxygen atoms from the system, the calculated formation energy per oxygen vacancy is gradually increased to ~5.5 eV and no abrupt change can be observed.

3.2.2. Structural evolution of oxygen-deficient $LaFeO_3$

It was previously reported that $LnCoO_3$ (Ln = La - Eu) can be continuously reduced in a hydrogen atmosphere with the formation of a series of oxygen-deficient perovskite structures [41]. Therefore, upon formation of oxygen vacancies, the crystal structures of $LaMO_3$ must undergo an evolution arising from the displacement of the remaining ions. In stoichiometric $LaMO_3$, each M cation is surrounded by six oxygen anions in an octahedral geometry while each La cation is surrounded by eight corner-sharing MO_6 octahedra. When an oxygen atom is removed, the local geometry around the vacancy would be significantly affected by the preference for certain polyhedral coordination geometry. Typically, the coordination number of the M cations would change to 5 (in square-based pyramid) and 4 (in tetrahedral or square planar geometries). Hence, these coordination geometries are of central importance when exploring the evolution of the crystal structures of $LaMO_{3-\delta}$ during the successive oxygen loss.

As for $LaFeO_3$, when removing the first or second oxygen atom, two octahedra that share the oxygen atom at the corner are transformed into two square-based pyramids (see Fig. 4), indicating that the tetrahedral coordination geometry is energetically less favorable under these circumstances. When the third and fourth oxygen vacancies are formed, however, the situation becomes quite different. A corner O atom shared by an octahedron and a square-based pyramid is most likely to be removed, leading to the formation of a tetrahedron which results from the abstraction of an equatorial and an apical oxygen atom from the initial FeO_6 octahedron. At the oxygen deficiency of 0.625, the most stable $LaFeO_{2.375}$ is formed by removing a corner O atom shared by two square-based pyramids, giving rise to a tetrahedron and a square planar geometry.

Interestingly, this predicted structural evolution upon oxygen vacancy formation in $LaFeO_3$ can be well reproduced by the experimental observations for $SrFeO_3$ [40]. At low temperatures and low oxygen deficiencies, the Fe cations prefers the square-based pyramidal coordination, and both $Sr_8Fe_8O_{23}$ ($SrFeO_{2.875}$) and $Sr_4Fe_4O_{11}$ ($SrFeO_{2.75}$) adopt ordered structures consisting of FeO_6 octahedrons and FeO_5 square-based pyramids. When the defect concentration is increased, the central Fe cation becomes tetrahedrally coordinated to the surrounding O atoms. For $SrFeO_{2.5}$, its high-temperature structure comprises octahedral, square-based pyramidal, and tetrahedral coordination geometries arranged in a random fashion. An atomistic simulation by Bakken et al. [42] indicated that at even higher temperatures the oxygen-deficient configurations containing the square planar FeO_4 geometry or the Fe cations with even lower coordination numbers are much higher in energy, which agrees well with our calculations that the presence of the square planar FeO_4 coordination in $LaFeO_{2.375}$ would lead to a sharp rise in energy at the oxygen deficiency of 0.625.

3.2.3. Maximum possible oxygen deficiency in $LaMO_3$

As demonstrated above, the structural stability of oxygen-deficient $LaFeO_{3-\delta}$ is closely related to the oxygen content in bulk oxide.

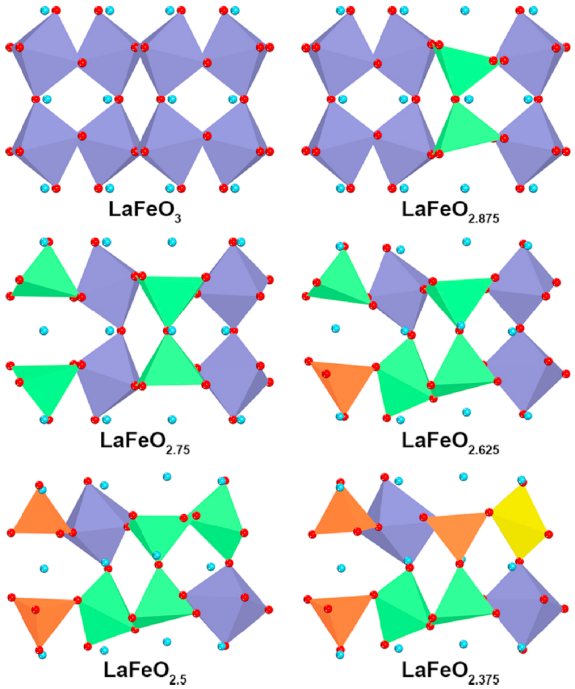

Fig. 4. Optimized structures of $LaFeO_{3-\delta}$ (δ = 0–0.625) upon successive removal of oxygen atoms. Octahedron, square-based pyramid, tetrahedron, and square planar geometry are shaded royal, green, orange, and yellow, respectively (For interpretation of the references to colour in this figure legend, the reader is referred to the web version of this article).

Likewise, while $LaMO_3$ (M = Mn, Co, Ni, and Cu) can be readily reduced to produce defective perovskites at low oxygen deficiency, there must exist a maximum possible oxygen deficiency before their crystal structures break up and the degree to which the perovskites can be reduced would depend very much on the electronic structures of the transition metal cations.

The calculated formation energies per oxygen vacancy ($\Delta E^{\delta}_{formation,vac}$) in $LaMO_{3-\delta}$ (M = Sc - Cu) as a function of the oxygen deficiency are presented in Fig. 5. It can be seen that for the first four perovskites [$LaMO_3$, M = (Sc - Cr)], all the $\Delta E^{\delta}_{formation,vac}$ is higher than 5.0 eV and there is no abrupt change along each "downhill" curve. Given the fact that it is hardest for them to be reduced in the stoichiometric structure, $LaMO_3$ (M = Sc - Cr) cannot be used as a catalyst in redox reactions even at a very high oxygen content. In contrast, the calculated $\Delta E^{\delta}_{formation,vac}$ in $LaMO_3$ (M = Mn - Cu) is below 5 eV at low oxygen deficiencies. However, when the oxygen concentration in bulk oxide is lowered to a specific value, additional oxygen removal would lead to a sharp increase in the $\Delta E^{\delta}_{formation,vac}$, which defines the maximum possible oxygen deficiency and reflects the tendency of the $LaMO_3$ perovskites to collapse into mixed binary oxides. From Fig. 5, one can see that in $LaMO_{3-\delta}$ (M = Mn - Ni) and $LaCuO_{3-\delta}$, the maximum possible oxygen deficiency is 0.5 and 1.0, respectively; that is, M^{3+} (M = Mn - Ni) can be possibly reduced to M^{2+} and $LaCuO_3$ may lose at most one lattice oxygen atom per formula unit before it is deactivated.

Experimentally, Fierro et al. studied the reduction of $LaMnO_3$ in H_2 and found the reduction process starts at 755 K and the degree of reduction is approximately 1 e^- per molecule at 1100 K [43], signifying the reduction of Mn^{3+} to Mn^{2+}. XRD has been performed to reveal the reversible phase transition of $LaFeO_3$ perovskite to mixed oxides in partial methane oxidation by chemical looping [7]. Both Fe^{2+} and Fe^{3+} were observed in the reduced perovskites, and the ratio between Fe^{2+}/Fe^{3+} was estimated based on the amount of oxygen removed. It was suggested that the maximum removable oxygen amount in $LaFeO_3$ corresponds to the reduction of Fe^{3+} to Fe^{2+} and the reducibility of Fe^{2+} is very low. In addition, Royer et al. [44] proposed a mechanism for $LaCoO_3$ reduction, showing that the Co^{3+} is first reduced to Co^{2+}, followed by the reduction of the Co^{2+} to Co° and the collapse of the perovskite structures, implying that the intermediate oxygen-deficient compound containing Co^{2+} cations is a stable structure during the removal of oxygen atoms. A two-step reduction of $LaNiO_3$ was observed by Falcón et al. using TPR [45]. It was reported that at low temperature the formation of the brownmilerite structure is due to the reduction of Ni^{3+} to Ni^{2+}. More recently, Touahra et al. [46] found that the reduction of $LaCuO_3$ also takes place in two steps. In the first step, however, Cu^{3+} is reduced to Cu^{+} rather than Cu^{2+} at 364 °C. In the second step, $LaCuO_2$ is decomposed into Cu° and La_2O_3 when heated to 506 °C.

The aforementioned experimental findings provide direct evidence in support of the existence of a maximum possible oxygen deficiency in the $LaMO_3$ structures. When an oxygen atom is removed from the lattice, the electrons left behind will be transferred to the remaining ions in the defective structure. As for $LaMO_3$ (M = Mn - Ni), when the δ reaches its maximum possible value of 0.5, the M cations are partially reduced and their oxidation states are decreased from +3 to the +2. By comparison, $LaCuO_3$ has its oxidation number reduced from +3 to +1 before the crystal structure breaks up. Therefore, transition metal needs to have at least two accessible oxidation states to maintain the stability of the oxygen-deficient perovskite structures during redox reactions. The reasoning behind the different behaviors between $LaMO_3$ (M = Mn - Ni) and $LaCuO_3$ is that although the M cations (M = Mn - Cu) all have the most frequently seen oxidation states of +2, which is due to the loss of the two outer 4 s electrons, Cu has an additional oxidation state of

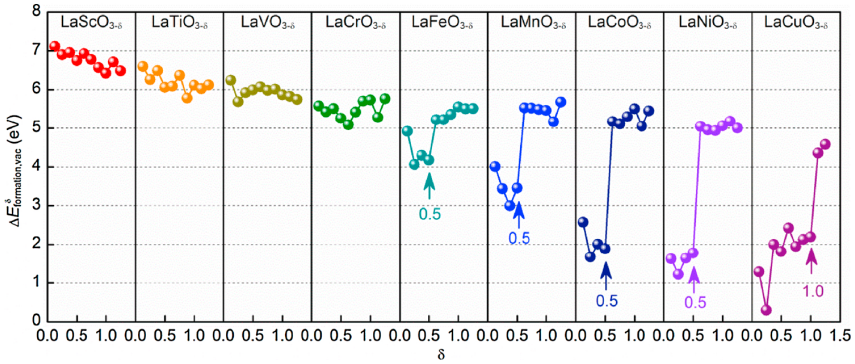

Fig. 5. Formation energy per oxygen vacancy ($\Delta E^{\delta}_{formation,vac}$) in $LaMO_{3-\delta}$ (M = Sc - Cu) as a function of oxygen deficiency.

+1 that may achieve a particularly stable $3d^{10}$ electronic configuration.

4. Conclusion

In this contribution, we have carried out DFT + U calculations to explore the reducibility and structural stability of $LaMO_3$ (M = Sc - Cu). With the exception of $LaFeO_3$, the calculated formation energy of the first oxygen vacancy decreases gradually from $LaScO_3$ to $LaCuO_3$, which can be used to gauge their reducibility. The first four $LaMO_3$ perovskites that have very high oxygen vacancy formation energies can hardly be reduced under mild conditions, while the other five perovskites have much better redox properties. The calculated bonding energies that measure the direct transition metal-oxygen interactions vary in much the same way as the oxygen vacancy formation energies, and the distortion energy is dependent strongly on the displacement of the remaining ions. When oxygen atoms are removed from the oxides, the nearest neighbor transition-metal cations to the vacancies are the primary acceptors of the electrons left behind.

When multiple oxygen vacancies are present in bulk oxide, the calculated oxygen vacancy formation energy rises sharply at a certain oxygen deficiency, which defines the degree to which the $LaMO_3$ perovskites can be reduced. In $LaMO_{3-\delta}$ (M = Mn - Ni) and $LaCuO_{3-\delta}$, the maximum possible values are 0.5 and 1.0, respectively; that is, M^{3+} (M = Mn - Ni) can be possibly reduced to M^{2+} and $LaCuO_3$ may lose at most one lattice oxygen atom per formula unit before it is deactivated. From the variation in the oxidation states of the transition metals, it can be concluded that only when transition metals have more than one accessible and commonly seen oxidation state may oxygen be successively removed from the corresponding perovskites while retaining their crystal structures.

Acknowledgements

This work is supported by the Natural Science Foundation of China (21473053, 91645122, and U1663221), the National Key Research and Development Program of China (2018YFB0604700), and the Fundamental Research Funds for the Central Universities (222201718003). The computational time provided by the Notur project is highly acknowledged.

Appendix A. Supplementary data

Supplementary material related to this article can be found, in the online version, at doi:https://doi.org/10.1016/j.cattod.2018.04.070.

References

[1] M.A. Pena, J.L.G. Fierro, Chem. Rev. 101 (2001) 1981–2018.
[2] S. Royer, D. Duprez, F. Can, X. Courtois, C. Batiot-Dupeyrat, S. Laassiri, H. Alamdari, Chem. Rev. 114 (2014) 10292–10368.
[3] S. Gupta, M.K. Mahapatra, P. Singh, Mater. Sci. Eng. R. 90 (2015) 1–36.
[4] S.B. Adler, Chem. Rev. 104 (2004) 4791–4844.
[5] J.W. Fergus, Sensor Actuat, B Chem. 123 (2007) 1169–1179.
[6] O. Mihai, D. Chen, A. Holmen, Ind. Eng. Chem. Res. 50 (2011) 2613–2621.
[7] O. Mihai, D. Chen, A. Holmen, J. Catal. 293 (2012) 175–185.
[8] E. Fabbri, D. Pergolesi, E. Traversa, Chem. Soc. Rev. 39 (2010) 4355–4369.
[9] M. Pavone, A.M. Ritzmann, E.A. Carter, Energy Environ. Sci. 4 (2011) 4933–4937.
[10] L.M. Petkovic, V. Utgikar, S.N. Rashkeev, J. Phys. Chem. C 115 (2011) 8709–8715.
[11] T. Nakamura, G. Petzow, L.J. Gauckler, Mater. Res. Bull. 14 (1979) 649–659.
[12] K. Kamata, T. Nakajima, T. Nakamura, Mater. Res. Bull. 14 (1979) 1007–1012.
[13] K. Kamata, T. Nakajima, T. Hayashi, T. Nakamura, Mater. Res. Bull. 13 (1978) 49–54.
[14] J.M.D. Tascón, L. González Tejuca, React. Kinet. Catal. Lett. 15 (1980) 185–191.
[15] O. Garlea, C. Darie, C. Bougerol, O. Isnard, P. Bordet, Solid State Sci. 5 (2003) 1095–1104.
[16] F. Dong, Y. Chen, D. Chen, Z. Shao, ACS Appl. Mater. Interfaces 6 (2014) 11180–11189.
[17] M.M. Kuklja, E.A. Kotomin, R. Merkle, Y.A. Mastrikov, J. Maier, Phys. Chem. Chem. Phys. 15 (2013) 5443–5471.
[18] K. Maiti, J. Fink, S. de Jong, M. Gorgoi, C. Lin, M. Raichle, V. Hinkov, M. Lambacher, A. Erb, M.S. Golden, Phys. Rev. B 80 (2009) 165132.
[19] C. Zhang, P.D. Bristowe, RSC Adv. 3 (2013) 12267–12274.
[20] G. Kresse, J. Hafner, Phys. Rev. B 47 (1993) 558–561.
[21] G. Kresse, J. Furthmiiller, Phys. Rev. B 54 (1996) 11169–11186.
[22] J.P. Perdew, K. Burke, M. Ernzerhof, Phys. Rev. Lett. 77 (1996) 3865–3868.
[23] G. Kresse, D. Joubert, Phys. Rev. B 59 (1999) 1758–1775.
[24] J. Wellendorff, K.T. Lundgaard, A. Møgelhøj, V. Petzold, D.D. Landis, J.K. Nørskov, T. Bligaard, K.W. Jacobsen, Phys. Rev. B 85 (2012) 235149.
[25] V.I. Anisimov, F. Aryasetiawan, A.I. Lichtenstein, J. Phys. Condens. Matter 9 (1997) 767–808.
[26] V.I. Anisimov, J. Zaanen, O.K. Andersen, Phys. Rev. B 44 (1991) 943–954.
[27] H.J. Monkhorst, J.D. Pack, Phys. Rev. B 13 (1976) 5188–5192.
[28] K. Knížek, Z. Jirák, J. Hejtmánek, P. Novák, J. Phys. Condens. Matter 18 (2006) 3285.
[29] K. Nomura, H. Kageyama, K. Ohmi, M. Fujita, T. Ueda, Chem. Lett. 42 (2013) 1268–1270.
[30] R. van Grieken, J.L. Peña, A. Lucas, G. Calleja, M.L. Rojas, J.L.G. Fierro, Catal. Lett. 8 (1991) 335–344.
[31] S. Royer, D. Duprez, ChemCatChem 3 (2011) 24–65.
[32] A. Evdou, V. Zaspalis, L. Nalbandian, Fuel 89 (2010) 1265–1273.
[33] N. Orlovskaya, D. Steinmetz, S. Yarmolenko, D. Pai, J. Sankar, J. Goodenough, Phys. Rev. B 72 (2005) 1–7.
[34] S. Gangopadhyay, T. Inerbaev, A. Masunov, D. Altilio, N. Orlovskaya, J. Mesit, R. Guha, A. Sleiti, J. Kapat, ACS Appl. Mater. Interfaces 1 (2009) 1512–1519.
[35] H. Kang, J.L. Beauchamp, J. Am. Chem. Soc. 108 (1986) 5663–5668.
[36] E.R. Fisher, P.B. Armentrou, J. Phys. Chem. 94 (1990) 1674–1683.
[37] C.W. Bauschlicher, P. Maitre, Theor. Chim. Acta 90 (1995) 189–203.
[38] R.F.W. Bader, T.T. Nguyen-Dang, Y. Tal, Rep. Prog. Phys. 44 (1981) 893–948.
[39] J.B. Goodenough, Magnetism and the Chemical Bond, Interscience Publishers, New York, 1963.
[40] S. Stolen, E. Bakken, C.E. Mohn, Phys. Chem. Chem. Phys. 8 (2006) 429–447.
[41] T. Arakawa, N. Ohara, J. Shiokawa, J. Mater. Sci. 21 (1986) 1824–1827.
[42] E. Bakken, N.L. Allan, T.H.K. Barron, C.E. Mohn, I.T. Todorov, S. Stølen, Phys. Chem. Chem. Phys. 5 (2003) 2237–2243.
[43] J.L.G. Fierro, J.M.D. Tascón, L.G. Tejuca, J. Catal. 89 (1984) 209–216.
[44] S. Royer, H. Alamdari, D. Duprez, S. Kaliaguine, Appl. Catal. B Environ. 58 (2005) 273–288.
[45] H. Falcón, M.J. Martínez-Lope, J.A. Alonso, J.L.G. Fierro, Solid State Ionics 131 (2000) 237–248.
[46] F. Touahra, A. Rabahi, R. Chebout, A. Boudjemaa, D. Lerari, M. Sehailia, D. Halliche, K. Bachari, Int. J. Hydrogen Energy 41 (2016) 2477–2486.